Journal of Heat and Mass Transfer Research

Journal homepage: https://jhmtr.semnan.ac.ir

Semnan University

ISSN: 2383-3068

Research Article

Double diffusion mixed convection in a porous cylindrical cavity filled with a Casson nanofluid driven by a lid, taking into account the Soret and Dufour effects

Mustapha El hamma [a]*, Lebna Elattari[a], Soufiane Nouari[b]

[a] *Department of Physics, Team of Modeling and Simulation in Mechanics and Energetics (MSME), Faculty of Sciences, Mohammed V University in Rabat, Morocco.*

[b] *Laboratory Mechanics, Processes, Energy and Environment(LMPEE),Ensa Agadir .*

ARTICLE INFO

Article history:

Received:

Revised:

Accepted:

Keywords:

Mixed convection;

Darcy regime ;

Casson nanofluid;

Soret effect and Dufour ;

Thermosolutal.

ABSTRACT

The aim of this study is to analyze and calculate the thermosolutal mixed convection in a porous cylindrical cavity containing a Casson nanofluid (aluminum nanoparticle). This research was conducted under Darcy regime conditions with $R_{e,nf} < 10$. Analysis is carried out for a range of model factors including Richardson's number (0.1 to 1), Reynolds number (1 to 9), porosity (0.1 to 1), Soret and Dufour numbers (0.1 to 1), Casson fluid parameter (0.1 to 0.5), Buoyancy ratio (1 to 10), Prandtl number (1 to 10), and Geometric aspect ratio (2 to 3). The volume fraction of nanoparticles was set at $\varphi = 5\%$ for the flow of Casson nanofluid through porous layers, as explained by the extended Brinkman-Forchheimer DARCY law. As we note in this research that the thermosolutal transfer decreases with the increase in Richardson number in the case of $R_{i,nf}$ >10 and the thermosolutal transfer increases with the increase in casson fluid parameter, on the contrary we notice that the transfer of heat decreases with the increase in the Soret and Dufour numbers, and at the end we find that thetmosolutal transfer increases with the increase in Reynolds number in the Dacian regime. Numerical simulations were conducted using numerical methods rooted in the finite volume method (FVM). Fortran numerical codes using FVM were implemented in the experiments to achieve the results. Therefore, we examined how various factors impact both heat transfer and concentration rate.

1. Introduction

Understanding thermosolutal mixed convection is important for various scientific and engineering applications, as it enables the solution of complex issues and the advancement of more efficient and sustainable technologies in areas like solar ponds, materials processing, drug delivery systems, cancer treatments, solar air conditioning, electronics packaging, and food processing, etc. [1-2]. This effect is of great interest to scientific experimenters modeling double diffusion mixed convection phenomena. The exploration carried out to model the miracle of mixed convection or double diffusion is different and focuses on understanding the abecedarian mechanisms of heat and mass transfer. thus, you can cite the ensuing works :

* **Corresponding author.**
E-mail address: *Mustapha_elhamma@um5.ac.ma*

Cite this article as:
El Hamma, M., Elattari,L,.Nouari,S ,.2024. Double diffusion mixed convection in a porous cylindrical cavity filled with a Casson nanofluid driven by a lid, taking into account the Soret and Dufour effects. *Journal of Heat and Mass Transfer Research*, 11(2), pp. xx-xx.
https://doi.org/10.22075/JHMTR.2024.39315.2050

s. sivasankaran et al [3] were fascinated by twofold dissemination blended convection in a depth driven by a top with non-uniform warming on the side dividers. M. Bhuvaneswari et al [4] carried out a numerical consider on twofold dissemination blended convection with Soret impact in a depth driven by a two-sided cover. P. M. Guimarãesa et al [5] inspected blended convection in a ventilated square depression utilizing nanofluid. T. Hayat et al [6] were curious about the stagnation point stream by blended convection of the Casson liquid with convection boundary conditions. M. A. Teamah et al [7] carried out a numerical think about of a blended convective stream with twofold dissemination in a rectangular walled in area with an protects moving cover. K. Khanafer et al [8] examined the phenomenon of double diffusive mixed convection in a lidded enclosure filled with a fluid saturated permeable medium. T. Jamir et al [9] carried out a consider on Impacts of radiation absorption, Soret and Dufour on an unsteady MHD mixed convective stream past a vertical porous plate with sliding condition and viscous dissipation. M. El Hamma et al [10] carried out a think about on thermosolutal convection in a cylindrical permeable cavity filled with a nanofluid and taking into consideration the Soret and Dufour impacts. A. Mahdy [11] inspected the Soret and Dufour Impact on double diffusion mixed convection from a vertical surface in a porous medium immersed with a non-Newtonian liquid. P. Mondal et al [12] carried out a think about of mixed convection with double diffusion and entropy generation of nanofluid in a trapezoidal depth. S. Moolya, et al [13] carried out a think about on the Part of magnetic field and cavity inclination on mixed double diffusion convection in a closed rectangular space. M. El Hamma et al [14] were curious about thermosolutal convection in a permeable cylindrical cavity filled with a Casson nanofluid, taking into consideration the Soret and Dufour impacts. N. Guerroudj et al [15] they carried out an in-depth ponder on Ferrohydrodynamics Mixed convection of a ferrofluid in a vertical channel with permeable squares of different shapes. N. S. Wahid et al [16] think about the stream of mixed convection magnetic nanofluids before a rotating vertical permeable cone. A. Bouras et al [17] were fascinated by the 3D numerical recreation of turbulent mixed convection in a cubic cavity containing a hot square. Z.H. Khan et al [18] they carried out Thermal treatment inside a partially heated triangular cavity filled with casson fluid with an inner cylindrical obstacle via FEM approach. M. Hamid et al [19] were curious about Characterizing natural convection and thermal behavior in a square cavity with curvilinear corners and central circular obstacles. B.A.I Bendrer [20] carried out a think about of 3D magnetic buoyancy-driven flow of hybrid nanofluids confined wavy cubic enclosures including multi-layers and heated obstacle. S. E. Ahmed [21] examined the Dissipated-radiative compressible flow of nanofluids over unsmoothed inclined surfaces with variable properties.

The originality of the display work is the modeling of mixed thermosolutal convection in a permeable cylindrical cavity filled with a Casson nanofluid driven by a cover beneath the impact of the thermo-diffusion phenomenon (Soret and Dufour impact).

2. Description of The Problem And Governing Equations

2.1 Detail the problem

The phenomenon of mixed double diffusion convection convection was considered in a porous cylindrical enclosure filled and saturated by a Casson nanofluid driven by an upper cover. The enclosure in address (Fig.1) has lower and upper bases subjected, individually, to uniform temperatures and concentrations. The sidewalls are accepted adiabatic and impermeable.

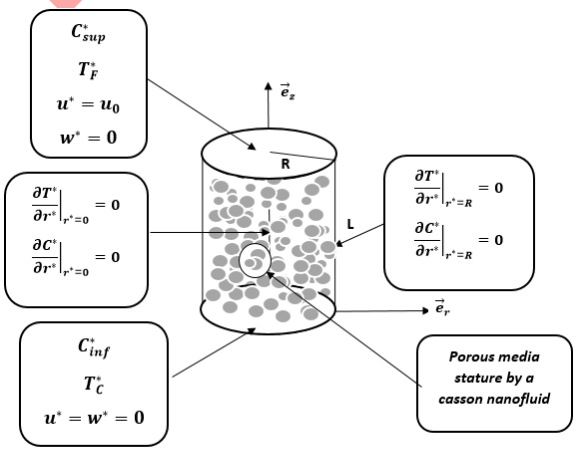

Fig. 1. Geometry of the studied problem

2.2 Governing Equations

The Governing Equations deciphering the phenomenon examined are based on the conservation equations of continuum mechanics. (Equation of continuity, quantity of movement, conservation of energy and mass). Hence, the Darcy-Brinkman-Forchheimer laws depict the stream of the nanofluid within the porous layers. The thermo-physical properties of the nanofluid

are expected constant. Conditions in dimensional shape are composed.

$$\frac{1}{r^*}\frac{\partial(r^*u^*)}{\partial r^*}+\frac{\partial w^*}{\partial z^*}=0 \qquad (1)$$

$$\begin{aligned}\frac{1}{\varepsilon^2}\left(\frac{1}{r^*}\frac{\partial(r^*u^*\Omega^*)}{\partial r^*}+\frac{\partial(w^*\Omega^*)}{\partial z^*}-\frac{u^*\Omega^*}{r^*}\right)&=-\frac{\mu_{nf}}{K\rho_{0nf}}\Omega^*\\&-\frac{\rho_0(1-\varphi)}{\rho_{0nf}}\beta_T\, g\frac{\partial T^*}{\partial r^*}\\&-\frac{\rho_0(1-\varphi)}{\rho_{0nf}}\beta_s\, g\frac{\partial C^*}{\partial r^*}\\&+\frac{\mu_{nf}}{\varepsilon\,\rho_{0nf}}\left(1+\frac{1}{\beta}\right)\left(\frac{\partial^2\Omega^*}{\partial r^{*2}}\right.\\&\left.+\frac{1}{r^*}\frac{\partial\Omega^*}{\partial r^*}+\frac{\partial^2\Omega^*}{\partial z^{*2}}-\frac{\Omega^*}{r^{*2}}\right)\\&-\frac{C_F}{K^{\frac{1}{2}}}\left|\vec{V}^*\right|\Omega^*\\&+\frac{C_F}{K^{\frac{1}{2}}}\left(w^*\frac{\partial\left|\vec{V}^*\right|}{\partial r^*}\right.\\&\left.-u^*\frac{\partial\left|\vec{V}^*\right|}{\partial z^*}\right)\end{aligned} \qquad (2)$$

$$\begin{aligned}\left(\frac{\partial(u^*T^*)}{\partial r^*}+\frac{\partial(w^*T^*)}{\partial z^*}+\frac{u^*T^*}{r^*}\right)&=\alpha\left(\frac{\partial^2T^*}{\partial r^{*2}}+\frac{\partial^2T^*}{\partial z^{*2}}+\frac{1}{r^*}\frac{\partial T^*}{\partial r^*}\right)\\&+\varepsilon\,N_{TC}\left(\frac{\partial^2C^*}{\partial r^{*2}}+\frac{\partial^2C^*}{\partial z^{*2}}\right.\\&\left.+\frac{1}{r^*}\frac{\partial C^*}{\partial r^*}\right)\end{aligned} \qquad (3)$$

$$\begin{aligned}\left(\frac{\partial(u^*C^*)}{\partial r^*}+\frac{\partial(w^*C^*)}{\partial z^*}+\frac{u^*C^*}{r^*}\right)&=D\,\varepsilon\left(\frac{\partial^2C^*}{\partial r^{*2}}+\frac{\partial^2C^*}{\partial z^{*2}}+\frac{1}{r^*}\frac{\partial C^*}{\partial r^*}\right)\\&+\varepsilon\,N_{CT}\left(\frac{\partial^2T^*}{\partial r^{*2}}+\frac{\partial^2T^*}{\partial z^{*2}}\right.\\&\left.+\frac{1}{r^*}\frac{\partial T^*}{\partial r^*}\right)\end{aligned} \qquad (4)$$

$$\Omega^*=\left(\frac{\partial u^*}{\partial z^*}-\frac{\partial w^*}{\partial r^*}\right) \qquad (5)$$

By introducing the following dimensionless quantities:

$$\mathrm{r}=\frac{\mathrm{r}^*}{\mathrm{R}}\qquad \mathrm{z}=\frac{\mathrm{z}^*}{\mathrm{R}},\mathrm{U}=\frac{\mathrm{u}^*}{u_0}\ ,\qquad \mathrm{W}=\frac{\mathrm{w}^*}{u_0}\ ,\ \Omega=\frac{\Omega^*R}{u_0}\ ,\psi=\frac{\psi^*}{R^2u_0}\ ,\ \mathrm{T}=\frac{\mathrm{T}^*-\mathrm{T}_\mathrm{F}^*}{\mathrm{T}_\mathrm{C}^*-\mathrm{T}_\mathrm{F}^*}\ ,\ \mathrm{C}=\frac{\mathrm{C}^*-\mathrm{C}_\mathrm{sup}^*}{\mathrm{C}_\mathrm{inf}^*-\mathrm{C}_\mathrm{sup}^*}$$

The previously established equations are written in dimensionless form:

$$\frac{1}{r}\frac{\partial(rU)}{\partial r}+\frac{\partial W}{\partial z}=0 \qquad (6)$$

$$\begin{aligned}\frac{1}{\varepsilon^2}\left(\frac{1}{r}\frac{\partial(rU\Omega)}{\partial r}+\frac{\partial(W\Omega)}{\partial z}-\frac{U\Omega}{r}\right)&=-\frac{1}{R_{e,nf}Da}\Omega\\&-R_{i,nf}\left(\frac{\partial T}{\partial r}+N\frac{\partial C}{\partial r}\right)\\&+\frac{1}{\varepsilon R_{e,nf}}\left(1+\frac{1}{\beta}\right)\left(\frac{\partial^2\Omega}{\partial r^2}+\frac{1}{r}\frac{\partial\Omega}{\partial r}\right.\\&\left.+\frac{\partial^2\Omega}{\partial z^2}-\frac{\Omega}{r^2}\right)-\frac{C_F}{\sqrt{Da}}\left|\vec{V}\right|\Omega\\&+\frac{C_F}{\sqrt{Da}}\left(W\frac{\partial\left|\vec{V}\right|}{\partial\bar{r}}\right.\\&\left.-U\frac{\partial\left|\vec{V}\right|}{\partial\bar{z}}\right)\end{aligned} \qquad (7)$$

$$\begin{aligned}\frac{\partial(\mathrm{UT})}{\partial\mathrm{r}}+\frac{\partial(\mathrm{WT})}{\partial\mathrm{z}}+\frac{\mathrm{UT}}{\mathrm{r}}&=\frac{1}{pr_{nf}R_{e,nf}}\left(\frac{\partial^2\mathrm{T}}{\partial\mathrm{r}^2}+\frac{\partial^2\mathrm{T}}{\partial\mathrm{z}^2}\right.\\&\left.+\frac{1}{\mathrm{r}}\frac{\partial\mathrm{T}}{\partial\mathrm{r}}\right)\\&+\frac{\varepsilon\,\mathrm{Du}}{pr_{nf}R_{e,nf}}\left(\frac{\partial^2\mathrm{C}}{\partial\mathrm{r}^2}+\frac{\partial^2\mathrm{C}}{\partial\mathrm{z}^2}\right.\\&\left.+\frac{1}{\mathrm{r}}\frac{\partial\mathrm{C}}{\partial\mathrm{r}}\right)\end{aligned} \qquad (8)$$

$$\begin{aligned}\frac{\partial(\mathrm{UC})}{\partial\mathrm{r}}+\frac{\partial(\mathrm{WC})}{\partial\mathrm{z}}+\frac{\mathrm{UC}}{\mathrm{r}}&=\frac{\varepsilon}{Sc_{nf}R_{e,nf}}\left(\frac{\partial^2\mathrm{C}}{\partial\mathrm{r}^2}+\frac{\partial^2\mathrm{C}}{\partial\mathrm{z}^2}\right.\\&\left.+\frac{1}{\mathrm{r}}\frac{\partial\mathrm{C}}{\partial\mathrm{r}}\right)\\&+\frac{\varepsilon\mathrm{Sr}}{Sc_{nf}R_{e,nf}}\left(\frac{\partial^2\mathrm{T}}{\partial\mathrm{r}^2}+\frac{\partial^2\mathrm{T}}{\partial\mathrm{z}^2}\right.\\&\left.+\frac{1}{\mathrm{r}}\frac{\partial\mathrm{T}}{\partial\mathrm{r}}\right)\end{aligned} \qquad (9)$$

$$\Omega=\left(\frac{\partial U}{\partial z}-\frac{\partial W}{\partial r}\right) \qquad (10)$$

The following dimensionless numbers are introduced:

$R_{e,nf} = \frac{u_0 R}{\upsilon_{nf}}$ (Reynolds number), $Da = \frac{K}{R^2}$ (Darcy number) , $R_{i,nf} = \frac{G_{T,nf}}{R_{e,nf}{}^2}$ (Richardson number), $N = \frac{\beta_s \Delta C}{\beta_T \Delta T} = \frac{G_{C,nf}}{G_{T,nf}}$ (Buoyancy ratio) ,$Sc_{nf} = \frac{\upsilon_{nf}}{D}$ (Schmidt number) , $Du = \frac{N_{TC}\,\Delta C}{\alpha\,\Delta T}$ (Dufour number) ,$Sr = \frac{N_{CT}\,\Delta T}{D\Delta C}$ (Soret number), $Pr_{nf} = \frac{\upsilon_{nf}}{\alpha_{nf}}$ (Prandtl number).

Here are the dimensionless boundary conditions of the selected problem

$r = 0,\ U = W = 0, \left.\frac{\partial T}{\partial r}\right|_{r=0} = 0,\ \left.\frac{\partial C}{\partial r}\right|_{r=0} = 0,$
$\Omega|_{r=0} = 0$

$r = 1, U = W = 0,$
$\left.\frac{\partial T}{\partial r}\right|_{r=1} = 0,\ \left.\frac{\partial C}{\partial r}\right|_{r=1} = 0,$
$\Omega|_{r=1} = 0$

$z = 0,\ U = W = 0,\ T = 1,\ C = 1, \Omega|_{z=0} = 0$

$z = A\,, U = 1, W = 0,\ ,\ T = 0,\ C = 0,\ \Omega|_{z=A} = 0$

The Nusselt average (Nu) and Sherwood (Sh) represent the heat and mass transfer on the active wall horizontally with the defined relationships

$$Nu = -2A\int_0^1 \left.\frac{\partial T}{\partial z}\right|_{z=0}$$

$$Sh = -2A\int_0^1 \left.\frac{\partial C}{\partial z}\right|_{z=0} dr$$

3. RESOLUTION PROCESS

The discretization of the governing equations was carried out by FVM utilizing uniform network sizes [22-23]. The algebraic form of the equations gotten, to which we include boundary conditions, are fathomed utilizing the double sweep method. The equations gotten after discretization were illuminated utilizing the FORTRAN code. The convergence basis is given by:

$$\frac{\sum_i \sum_j |f_{i,j}^{n+1} - f_{i,j}^{n}|}{\sum_i \sum_j |f_{i,j}^{n+1}|} \le 10^{-5}$$

To confirm the good behavior of the numerical model, the grid convergence test is carried out at different grid levels and by restricting $A = 2\,, \varepsilon = 0.4\,,\ N = 1, Pr_{nf} = 6.8,\ \beta = 1, R_{e,nf} = 1\,, \varphi = 0.05, Sc_{nf} = 1,\ Da = 0.001, Sr = 1,\ Du = 1$ and are presented in Table 1. For this purpose, the average heat fluxes are calculated. We see that the Sizes of the grid converge in the 141 × 141 grid, for this we Avon works in this study on the 141 × 141grid.

Table 1. Grid independency study

Size of the grid	Nu	Error %
101 × 101	3.15952742623	1.4
111 × 111	3.15507977829.	0.11
121×121	3.15163879707	9.8×10^{-3}
131 × 131	3.15132778717	9.6×10^{-3}
141 × 141	3.15102639820	

to validate this work we take values in this porange in order to adapt it to the work [14], $\frac{1}{R_{e,nf}Da} = \bar{\Lambda}\frac{Pr_{nf}}{Da} = \frac{6.8}{0.001}$, $R_{i,nf} = \bar{\Lambda}^2 R_{T,nf}\ Pr_{nf} = 10^4 \times 6.8,\ \frac{1}{R_{e,nf}} = \bar{\Lambda}\, Pr_{nf} = 6.8\,,$ $\frac{1}{pr_{nf}R_{e,nf}} = 1,\ \frac{1}{Sc_{nf}R_{e,nf}} = \frac{1}{Le} = \frac{1}{2.5}$. When we solve these equations based on the values of item[14] we get the following values $R_{e,nf} = 0.147, R_{i,nf} = 68 \times 10^4\ ,\ Sc_{nf} = 0.059,\ Da = 0.001.$ Table2 gives a comparison between this research and the article [14]

Table 2. Comparison of the numerical procedure with [14]

β	Nu [14]	Sh [14]	Nu (This study)	Sh (This study)
0.1	2.71589	2.67435	2.71419	2.67315
0.2	2.72472	2.68326	2.72252	2.6812
0.4	2.72808	2.68668	2.72206	2.68362
0.6	2.72913	2.68774	2.72703	2.68454
0.8	2.72964	2.68826	2.72654	2.6841
1	2.72995	2.68857	2.72655	2.68625

4. Results and discussion

4.1 Effect of variation of Richardson, Reynolds numbers and Casson fluid parameter

Figures 2 and 3 show the influence of the Richardson number, Reynolds number and the Casson fluid parameter on the heat and mass transfer for $A = 2, \varepsilon = 0.4, N = 1, Pr_{nf} = 6.8, \varphi = 0.05, Sc_{nf} = 1, Da = 0.001, Sr = 1, Du = 1$

The average Nusselt number, which remains unchanged for:

The first two curves β =0.1, $R_{e,nf}$ =1 and et β =0.5, $R_{e,nf}$ = 1 in the interval $R_{i,nf}$<6.

The second two curves $\beta = 0.1$, $R_{e,nf}$ = 5 β =0.5, $R_{e,nf}$ = 5 in the interval $R_{i,nf}$ <8

The third two curves β =0.1, $R_{e,nf}$ = 9 and β =0.5, $R_{e,nf}$ = 9 in the interval $R_{i,nf}$ <10

When the Richardson number exceeds the threshold, we see a decrease in the average Nusselt number. The results show that an increase in the Richardson number from 0.1 to 100 the heat transfer decreases, this decrease is different for different Reynold value and Casson fluid parameter that the Reynold value and β increases the rate of decrease heat transfer increases see table 3. We also see in the same figures that the heat and mass transfer increase with the increase in β. This increase results from the viscosity of the fluid which decreases as the amount of the Casson parameter increases, and this reduction in viscosity leads to better thermosolutal transfer. Do not forget that heat and mass transfer increase with increasing Reynold's number, causing an increase in the kinetic energy of the particles leading to a better thermosolutal transfer.

Table 3. Heat transfer rate for $R_{i,nf}$ (between 0.1 and 100)

Variable Values	heat transfer rate for $R_{i,nf}$ (between 0.1 and 100)
β =0.1, $R_{e\,nf}$ =1	-63,25%
β =0.5, $R_{e\,nf}$ = 1	-18,37%
β = 0,1, $R_{e\,nf}$ = 5	-11,13%
β =0.5, $R_{e\,nf}$ = 5	-3,2%
β =0.1, $R_{e\,nf}$ = 9	-5,53%
β =0.5, $R_{e\,nf}$ = 9	-1,54%

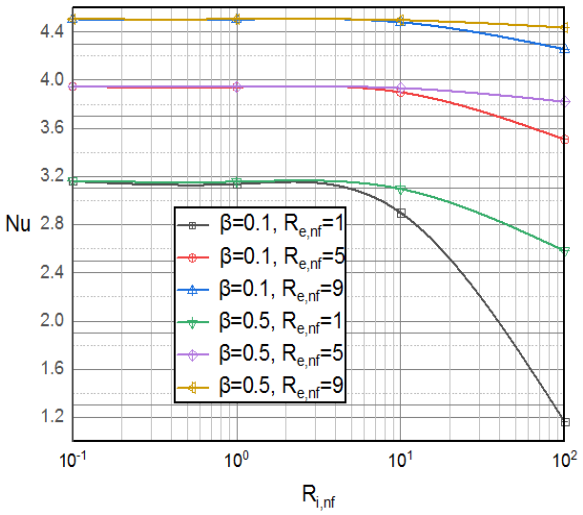

Fig. 2. The impact of $R_{i,nf}$, β and $R_{e,nf}$ on Nu

On the other hand, the average Sherwood number which remains unchanged for $R_{i,nf}$ <10 for the cases $R_{e,nf}$ = 1, for the other cases of Reynold number the variation threshold $R_{i,nf}$ =8. When the Richardson number exceeds its threshold, the average Sherwood number decreases. The results show that when the Richardson number increases from 0.1 to 100, the mass transfer decreases, this decrease is different from the Reynold value and the Casson flow parameter, and β this latter parameter increases the transfer rate of mass decreases, see Table 4.

Table 4. Mass transfer rate for $R_{i,nf}$ (between 0.1 and 100)

Variable Values	mass transfer rate For $R_{i,nf}$ (between 0.1 and 100)
β =0.1, $R_{e\,nf}$ =1	-32,64%
β =0.5, $R_{e\,nf}$ = 1	-24,31%
β = 0,1, $R_{e\,nf}$ = 5	-18,60%
β =0.5, $R_{e\,nf}$ = 5	-5,2%
β =0.1, $R_{e\,nf}$ = 9	-10,58%
β =0.5, $R_{e\,nf}$ = 9	-2,3%

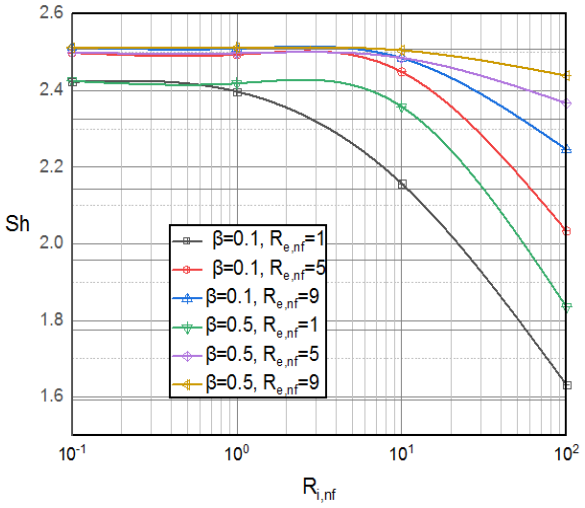

Fig. 3. The impact of $R_{i,nf}$, β and $R_{e,nf}$ on Sh

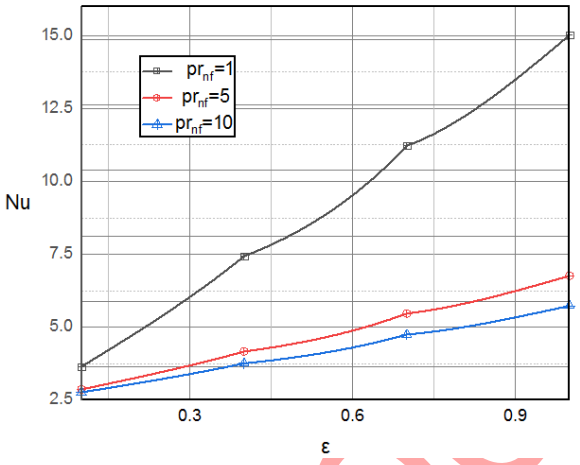

Fig. 4. The impact of ε and Pr_{nf} on Nu

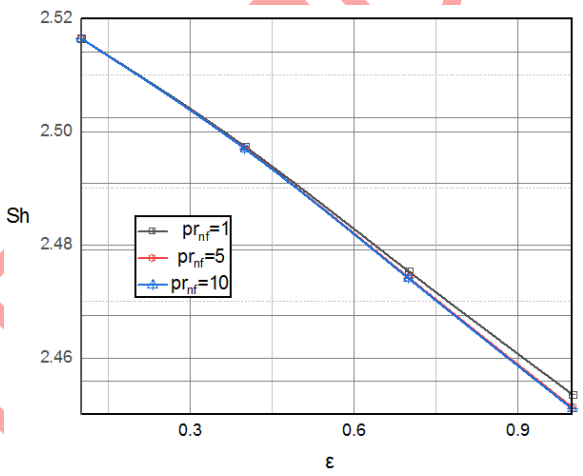

Fig. 5. The impact of ε and Pr_{nf} on Sh

4.2 Effect of variation in Porosity numbers and Prandtl number

Figures 4 and 5 respectively show the effect of Porosity and Prandtl numbers on heat and mass transfer.

We notice in Figure 4 that average Nusselt evolves monotonically with increasing Porosity. This increase results from the argument that thermal conductivity has with the increase in Porosity. We see in the same figures that the average Nusselt values decrease when the Prandtl number increases, this decrease results in the increase in Prandtl number improving the resistive force more than the thermal and solutal volume forces. In Figure 5, we represent the Porosity effect on mass transfer. We see in this figure that the average Sherwood value decreases with the increase in Porosity, this increase writing down the Permeability and decrease in Mass Diffusivity. Table 5 shows the heat and mass transfer rate for ε (between 0.1 and 1).

Table 5. Heat and mass transfer rate for ε (between 0.1 and 1)

Variable Values	heat transfer rate for ε (between 0.1 and 1)	mass transfer rate For ε (between 0.1 and 1)
$Pr_{nf} = 1$	75,8 %	-2,56 %
$Pr_{nf} = 5$	57,7%	-2,6 %
$Pr_{nf} = 10$	51,8%	-2,7 %

4.3 Effect of variation in Darcy, Soret and Dufour numbers

From Figure 6, it can be seen that the average Sherwood number decreases with the increase in Soret number, and the Soret number is estimated to be between 0.1 and 1. In contrast, the increase in Soret coefficient, which represents thermal diffusion phenomena, leads to a reduction in mass transfer. On the other hand the average Sherwood number which remains almost unchanged for $< 10^{-8}$. When the Darcy number exceeds this threshold $Da = 10^{-8}$ we see a decrease in the average Sherwood number with the increase in Da, which results from an increase in Permeability, which improves the thermosolutal resistive force . Table 6 shows the mass transfer rate for Da (between $Da = 10^{-8}$ and 1).

Table 6. Mass transfer rate for Da (between $10^{-10}$and 1)

Variable Values	mass transfer rate For Da (between $10^{-10}$and 1)
$Sr = 0{,}1$	-0,054%
$Sr = 0{,}5$	-0.053%
$Sr = 1$	-0.053%

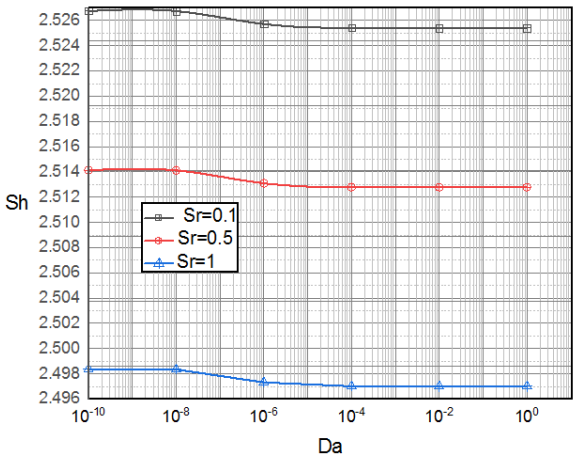

Fig. 6. The impact of Da and Sr on Sh

Figure 7 shows the Dufour effect on heat transfer. From this figure, we can see that the average value of Nusselt decreases as the Dufour number increases. This represents the phenomenon of thermal diffusion. As for the number of Darcy increases, the number of nusselt decreases. Table 7 shows the heat transfer rate for Da (between 10^{-10} and 1).

Table 7. Heat transfer rate for Da (between $10^{-10}$and 1)

Variable Values	heat transfer rate For Da (between $10^{-10}$and 1)
$Du = 0{,}1$	-0,052%
$Du = 0{,}5$	-0.041%
$Du = 1$	-0.032%

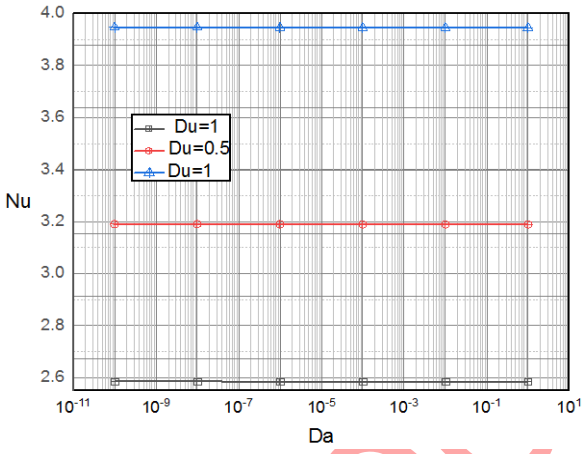

Fig.7. The impact of Da and Sr on Nu

4.4 Effect of varying Reynolds numbers, Buoyancy ratio and Geometric aspect ratio

Figures 8 and 9 show the influence of Reynolds numbers, Buoyancy ratio and Geometric aspect ratio on heat and mass transfer pour $\varepsilon = 0.4$, $R_{i,nf} = 1, Pr_{nf} = 6.8,\ \varphi = 0.05, Sc_{nf} = 1,$ $Da = 0.001, Sr = 1,\ Du = 1.$

In this study, we focused our attention on the flow in the Darcy regime for $R_{e,nf} < 10$.

We see in these figures that the heat and mass transfer increase with the increase in $R_{e,nf}$, This fact is proven by the fact that the kinetic energy of the particles improves with the increase in Reynolds number. While a contrary behavior We see on the same figures that transformation of heat and mass decreases with the increase of Buoyancy ratio and Geometric aspect ratio this decrease results that the increase in the numbers Buoyancy ratio and Aspect ratio geometric resistive force improvement more than thermal and solutal volume forces. Table 8 shows the heat and mass transfer rate for $R_{e,nf}$ (between 1 and 9).

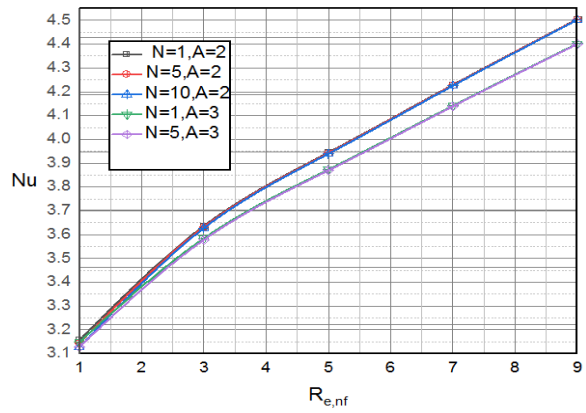

Fig. 8. The impact of $R_{e,nf}$, N and A on Nu

Table 8. Heat and masse transfer rate for $R_{e,nf}$ (between 1 and 9)

Variable Values	heat transfer rate For $R_{e,nf}$ (between 1 and 9)	mass transfer rate For $R_{e,nf}$ (between 1 and 9)
$N = 1\ , A = 2$	30%	3,7%
$N = 5\ , A = 2$	30,2%	4,1%
$N = 10\ , A = 2$	30,5%	4,7%
$N = 1\ , A = 3$	28.4%	1.4%
$N = 5\ , A = 3$	28,9%	2,2%

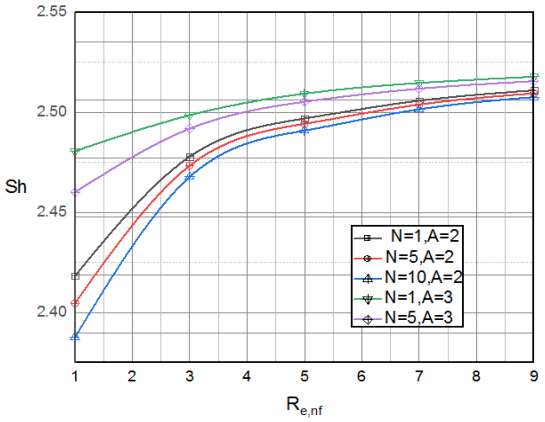

Fig.9. The impact of $R_{e,nf}$, N and A on Sh

5. Conclusions

This study focused on mixed thermosolutal convection in a cylindrical cavity driven by a lid, filled with a casson nanofluid, leading to the following conclusions:

Heat and mass transfers remain unchanged. When the Richardson number exceeds the threshold we see a decrease in the average Nusselt and average Sherwood numbers, we also see that the increase in the Casson parameter causes an increase in heat and mass transfer. This is explained by the importance of the flow intensity with increasing Casson fluid parameter. We notice that the heat transfer evolves monotonically with increasing Porosity. This increase results from the argumentation of thermal conductivity with the increase in Porosity. On the contrary the decrease in heat and mass transfer with the increase in Prandtl number. This decrease increases the resistive force more than the thermal and solute volume forces. We see that the average shrewood number decreases with increasing Porosity. This decrease results from the increase in

Permeability and decrease in Mass Diffusivity with the increase in Porosity. It can be seen that

the average Sherwood number, which remains almost, unchanged for $Da < 10^{-8}$. When the Darcy number exceeds this threshold, $Da = 10^{-8}$we see a decrease in the average Sherwood number with the increase in Da, which results from an increase in Permeability, which improves the thermosolutal resistive force. On the other hand, the average Sherwood number decreases with the increase in the Soret number. On the other hand, the increase in the Soret coefficient, which represents thermal diffusion phenomena, leads to a decrease in mass transfer. We also notice that Nusselt's average decreases with the increase in the Dufour and Darcy numbers. We notice that the heat transfer number and mass increase with the increase in Reynolds number. This increase results from the increase in the kinetic energy of the particles improved with the increase in Reynolds number. While a contrary behavior, it is observed that heat and mass transformation decreases with the increase of Buoyancy ratio and Geometric aspect ratio this decrease results that the increase in the numbers Buoyancy ratio and Geometric aspect ratio improvement of resistive force more than the thermal and solutal volume forces.

Nomenclature

A	Geometric aspect ratio $(\frac{L}{R})$
C^*	Concentration,[Kg/m^3]
$G_{C,nf}$	Grashof number concentration
$G_{T,nf}$	Grashof number temperature
C	Dimensionless concentration
Sc_{nf}	Schmidt number
C_F	Forchheimer coefficient
D	Mass diffusivity, [m^2/s]
Da	Darcy number
Du	Dufour number
K	Permeability of the porous medium, [m^2]
L	Cylinder height, [m]
R	Cylinder radius, [m]
r^*	Radial coordinate
r	Dimensionless radial coordinate
z^*	Axial coordinate
z	Dimensionless axial coordinate
N	Buoyancy ratio
N_{CT}	Soret coefficient, [Kg/m. K. s]
N_{TC}	Dufour coefficient, [m^5, K/Kg, s]
Nu	Average Nusselt number

Pr_{nf}	Prandtl number
$R_{e,nf}$	Reynolds number
$R_{i,nf}$	Richardson number
Sh	Average Sherwood Number
Sr	Soret number
T^*	Temperature, $[K]$
T	Dimensionless temperature
U^*	Radial component of velocity $[m/s]$
U	Dimensionless radial component of velocity
W^*	Axial component of velocity $[m/s]$
W	Dimensionless axial component of velocity
β	Casson fluid parameter
β_T	Thermal expansion coefficient, K^{-1}
β_s	Solute expansion coefficient, $[Kg, mol/\mathrm{l}]$
ρ_0	Reference density of the fluid, $[\,Kg.m^{-3}]$
μ_{nf}	Dynamic viscosity of the nanofluid, [Kg/ $m.$s]
υ_{nf}	Kinematic viscosity of the nanofluid, $[m^2/\mathrm{s}]$
φ	Volume fraction of nanoparticles
Ω^*	Component of the rotational vector of velocities
Ω	Component of the dimensionless rotational velocity vector
ε	Porosity
α	Thermal diffusivity of the saturated porous medium, $[m^2/\mathrm{s}]$

References

[1] S. Moolya, S. Anbalagan, N. R. Devi, R. Moolya, 2022. Magnetohydrodynamics and Aspect Ratio Effects on Double Diffusive Mixed Convection and Their Prediction: Linear Regression Model, Journal of Heat and Mass Transfer Research, 9, 169 – 188. 10.22075/JHMTR.2023.28029.1387

[2] El Hamma, M., Taibi, M., Rtibi, A., Gueraoui, K. and Bernatchou, M.,2022. Effect of magnetic field on thermosolutal convection in a cylindrical cavity filled with nanofluid, taking into account Soret and Dufour effects. JP Journal of Heat and Mass Transfer, 26, 1-26. http://dx.doi.org/10.17654/0973576322009

[3] S. Sivasankaran, S. S. Ananthan, M. Bhuvaneswari, A. K. Abdul Hakeem, 2017. Double-diffusive mixed convection in a lid-driven cavity with nonuniform heating on sidewalls, Sadhana ,42, 1929–1941. 10.1007/s12046-017-0735-4

[4] M. Bhuvaneswari , S. Sivasankaran, Y. J. Kim, 2011. Numerical Study on Double Diffusive Mixed Convection with a Soret Effect in a Two-Sided Lid-Driven Cavity, Numerical Heat Transfer, Part A: Applications: An International Journal of Computation and Methodology, 59, 543-560. 10.1080/10407782.2011.561077

[5] P. M. Guimarães, M. D. Ramos, G. J. Menon, 2019. Mixed convection study in a ventilated square cavity using nanofluids, Journal of Heat and Mass Transfer Research, 6, 143-153. 10.22075/jhmtr.2018.14640.1208

[6] T. Hayat, S. A. Shehzad, A. Alsaedi, M. S. Alhothuali, 2012. Mixed Convection Stagnation Point Flow of Casson Fluid with Convective Boundary Conditions, CHIN. PHYS. LETT, 29, 114704. 10.1088/0256-307X/29/11/114704

[7] M. A. Teamah, W. M. El-Maghlany, 2010. Numerical simulation of double-diffusive mixed convective flow in rectangular enclosure with insulated moving lid, International Journal of Thermal Sciences 49, 1625-1638. https://doi.org/10.1016/j.ijthermalsci.2010.04.023

[8] K. Khanafer, K. Vafai, 2002. Double-Diffusive Mixed Convection in a Lid-Driven Enclosure Filled With A Fluid Saturated Porous Medium, Numerical Heat Transfer, Part A, 42, 465-486. https://doi.org/10.1080/10407780290059657

[9] T. Jamir , H. Konwar, 2022. Effects of Radiation Absorption, Soret and Dufour on Unsteady MHD Mixed Convective Flow past a Vertical Permeable Plate with Slip Condition and Viscous Dissipation, Journal of Heat and Mass Transfer Research ,9 , 155- 168. 10.22075/JHMTR.2023.28693.1399

[10] El Hamma, M., Rtibi, A., Taibi, M., Gueraoui, K., Bernatchou, M., 2022. Theoretical and Numerical Study of Thermosolutal Convection in a Cylindrical Porous Cavity Filled with a Nanofluid and Taking into Account Soret and Dufour Effects. International Journal on Engineering Applications (I.R.E.A.), 10, 56-65. DOI: https://doi.org/10.15866/irea.v10i1.20809

[11] A. Mahdy, 2010. Soret and Dufour effect on double diffusion mixed convection from a vertical surface in a porous medium saturated with a non-Newtonian fluid, J. Non-Newtonian Fluid Mech. 165, 568–575. https://doi.org/10.1016/j.jnnfm.2010.02.013

[12] P. Mondal, T.R. Mahapatra, 2021. MHD double-diffusive mixed convection and entropy generation of nanofluid in a trapezoidal cavity, International Journal of Mechanical Sciences 208, 106665. https://doi.org/10.1016/j.ijmecsci.2021.106665

[13] S.v. Moolya, A. Satheesh, 2020. Role of magnetic field and cavity inclination on double diffusive mixed convection in rectangular enclosed domain, International Communications in Heat and Mass Transfer, 118, 104814. https://doi.org/10.1016/j.icheatmasstransfer.2020.104814

[14] M. El Hamma, I. Aberdane , M. Taibi, A. Rtibi , K. Gueraoui, 2023. Analysis of MHD Thermosolutal Convection in a Porous Cylindrical Cavity Filled with a Casson Nanofluid, Considering Soret and Dufour Effects, Journal of Heat and Mass Transfer Research 10 ,197 – 206.

doi.org/10.22075/JHMTR.2023.30532.1439

[15] N. Guerroudj, B. Fersadou, K. Mouaici, H. Kahalerras, 2023. Ferrohydrodynamics Mixed Convection of a Ferrofluid in a Vertical Channel with Porous Blocks of Various Shapes, , Journal of Applied Fluid Mechanics, 16, 131-145. 10.47176/JAFM.16.01.1314

[16] N. S. Wahid, N. Md Arifin, N. S. Khashi'ie, I. Pop, N. Bachok, M. E. Hafidz Hafidzuddin, 2022. Mixed Convection Magnetic Nanofluid Flow past a Rotating Vertical Porous Cone, Journal of Applied Fluid Mechanics, 15, 1207-1220. 10.47176/JAFM.15.04.1063

[17] A. Bouras, S. Bouabdallah, B. Ghernaout, M. Arıc, Y. Cherif ,E. Sassine, 2021. 3D Numerical Simulation of Turbulent Mixed Convection in a Cubical Cavity Containing a Hot Block, , Journal of Applied Fluid Mechanics, 14, 8691-8801. 10.47176/JAFM.14.06.32604

[18] Khan, Z.H., Usman, M., Khan, W.A. et al, 2022. Thermal treatment inside a partially heated triangular cavity filled with casson fluid with an inner cylindrical obstacle via FEM approach. Eur. Phys. J. Spec. Top. 231, 2683–2694 https://doi.org/10.1140/epjs/s11734-022-00587-6

[19] M. Hamid, M.Usman, W. A. Khan, R. U. Haq, Z. Tian, 2024. Characterizing natural convection and thermal behavior in a square cavity with curvilinear corners and central circular obstacles,Applied Thermal Engineering, 248, doi.org/10.1016/j.applthermaleng.2024.123133

[20] B.A.I Bendrer, Aissa Abderrahmane, Sameh E. Ahmed, Zehba A.S. Raizah, 2021. 3D magnetic buoyancy-driven flow of hybrid nanofluids confined wavy cubic enclosures including multi-layers and heated obstacle, International Communications in Heat and Mass Transfer, 126, doi.org/10.1016/j.icheatmasstransfer.2021.105431.

[21] Ahmed, S. E., Arafa, A. A. M., & Hussein, S. A. , 2023. Dissipated-radiative compressible flow of nanofluids over unsmoothed inclined surfaces with variable properties. Numerical Heat Transfer, Part A: Applications, 84, (5), 507–528, https://doi.org/10.1080/10407782.2022.2141389

[22] S.V. Patankar, Numerical heat transfert and fluid flow, Hemisphere, New York, 1980.

[23] A. Bounouar,K. Gueraoui, M. Taibi, A. Lahlou, M. Driouich, M. Sammouda,S. Men-La-Yakhaf , 2016. Numerical and Mathematical Modeling of Unsteady Heat Transfer within a Spherical Cavity: Applications Laser in Medicine, Contemporary Engineering Sciences, 9, 1183 – 1199